Vol. 45, No. 4 (2023) 604-617, DOI: 10.24874/ti.1495.06.23.08

Tribology in Industry

www.tribology.rs

RESEARCH

Effect of Process Parameters on the Solid Particle Erosion Resistance of Transparent Materials

Doğan Acar[a], Mohammad Hussain Danesh[a], Ömer Necati Cora[a,*]

[a]*Department of Mechanical Engineering, Karadeniz Technical University, 61080, Trabzon, Turkey.*

Keywords:

Solid particle erosion
Transparent materials
Polycarbonate
Plexiglass
Laminated glass
ASTM G76-13
MIL-STD-3033

* Corresponding author:

Ömer Necati Cora
E-mail: oncora@ktu.edu.tr, necaticora@gmail.com

Received: 9 June 2023
Revised: 13 July 2023
Accepted: 7 August 2023

A B S T R A C T

The solid particle erosion (SPE) performance of three different transparent materials, polycarbonate solid sheet, plexiglass (Polymethylmethacrylate (PMMA), and laminated glass was investigated. Erosion tests were performed under different impact angles (20°, 30°, 45°, 60°, and 90°) and impinging velocities (75, 150, and 200 m/s). As erodent particles, alumina (Al_2O_3) with 52 μm average diameter and silicon carbide (SiC), particles with two different dimensions (71, and 348 μm in diameters) were used. The results showed that polycarbonate specimens outperformed the other tested samples regardless of impact velocity and impinging angle conditions. When the erosion resistance of samples at 90° and 75 m/s is taken into consideration, the polycarbonate sheet was found to be at least 14 times more erosion resistant compared to plexiglass, and 23 times more resistant than the laminated glass materials. In addition, polycarbonate exhibited an incubation behavior at lower impact velocity, and with SiC erodent.

1. INTRODUCTION

Plexiglass and polycarbonate are high-performance thermoplastic materials that have been widely used in many engineering fields due to their relatively low cost, good transparency, and higher strength compared to conventional glass. Laminated or security glass, on the other hand, is used as a windshield in both the automotive industry and construction fields. It is formed by combining two sheet glasses with an intermediate adhesive layer (polyvinyl butyral: PVB). These transparent materials are subjected to solid particle erosion (SPE) in their working environment to a different extent. SPE is the progressive removal of material from the surfaces of the target material due to repeated impacts of erodent particles. It has been reported that SPE causes damage in various engineering applications such as turbine blades of power plants, aircraft, pipelines, several parts in the oil and rig industry, and motor vehicles [1,2]. Components exposed to SPE either lose their functionality or their lifetime is substantially decreased.

SPE is a complex process affected by various parameters such as particle impact angle, impact velocity, particle shape and dimension, and target

materials properties [3–5]. Attempts to understand the basic mechanisms of the erosion phenomenon started in the second half of the 20th century and have continued increasingly since then. The researchers' main interest was concentrated on conventional materials, especially metals [6–8]. Finnie [9], through detailed studies on erosive wear, contributed to the understanding of the SPE behavior of various materials significantly. According to his experimental results, the maximum erosion rate of ductile materials resulted in low-impingement angles between 15-30° and the minimum erosion rate obtained at a high-impingement angle, namely, at 90°. On the other hand, for brittle materials, the maximum erosion rate was obtained at a normal impingement angle (90°), and the minimum rate was noted in the range of 15-30° angles. Furthermore, the peak erosion rate for semi-ductile materials was recorded at an intermediate impingement angle (e.g., 45°-60°) [10,11]. The effect of several process parameters such as temperature, impact velocity, erodent size and surface characteristics, impact angle, and the target material were investigated by quite a few researchers in the literature [12–16]. Among all these parameters, impact angle and impact velocity were noted to be the most dominant parameters of erosive behavior [17,18].

The erosion behavior of polymeric materials extremely depends upon the nature of the resin. Thermosetting polymers, such as epoxy and phenolic resins show brittle behavior whereas the erosion behavior of thermoplastics is a ductile type [19]. Wang et al. [20] have observed the ductile behavior of ultrahigh molecular weight polyethylene (UHMWPE) against the erosion of coal powder and silicon dioxide as erodent particles. Walley et al. [21] have also reported a peak erosion rate at an impingement angle of 30° for the erosion behavior of PE, PP, and PEEK. Bagci et al. [22] studied erosion wear of glass fiber mat-based polyester laminate materials by impacting abrasive particles in different sizes (250, 500, and 1000 μm), at different velocities of (23, 34, and 53 m/s), and impingement angles (15, 30 45, 60 75, and 90°). It was observed that the maximum erosion rate was obtained at 30° which implies that the glass fiber mat-based polyester laminate displays ductile behavior. In addition, the remarkable increase in the erosion rate was correlated with particle sizes. In other words, a change in abrasive particle size had a higher impact on erosive wear rate than impact velocity.

To analyze the influence of erosion parameters on composite laminate, a comprehensive study was done by Amaro et al. [23] on the glass/epoxy laminates with different particle sizes (20 mesh, 24 mesh, and 54 mesh) of spherical corundum aluminum oxide at different stand-off distances of 75 mm, 100 mm, and 125 mm. The experiments were carried out at various impingement angles (10, 45, and 90°) with a constant pressure of 2 bar. The maximum weight loss was obtained at an impact angle of 90°. Increasing the distance between the nozzle and the target material decreased the weight loss and depth of the eroded area, as expected. The bigger the particle size higher the erosion rate, and the deeper the wear crater. Moreover, similar observations were reported in the study of the SPE behavior of various thermoplastic polymers by researchers. In another study by Arani et al. [24], the effect of Al_2O_3 spheres added to epoxy matrix composites on erosion was investigated. It was observed that the erosive wear resistance of neat epoxy was weaker than epoxy composites at oblique impact angles.

Finnie and Sheldon [25] observed a transition from brittle to ductile behavior with decreasing erodent particle size. They investigated the erosion performance of glass materials against silicon carbide (SiC) erodent particles with sizes of 120 mesh (127 μm), 500 mesh (21 μm), and 1000 mesh (9 μm), and at an impact velocity of 152.4 m/s. In the case of larger particles (120 mesh), brittle erosion was observed, and the maximum value of erosion rate was obtained at about 90°. When the erodent size is reduced to 1000 mesh, the erosion characteristic was changed from brittle to the typical ductile. Furthermore, 1000 mesh was noted as sufficiently small for the ductile behavior of glass observed even when the impact velocity was increased to 304.8 m/s. Kerim et al. [26] investigated the effect of sand size, impact velocity, and natural aging on the surfaces of solar mirrors through SPE tests. The natural aging tests were performed in two different sites (oceanside and desert). The test results revealed no degradation of mirrors but just surface erosion. By comparing the results of these two different conditions; under a controlled glass mirror, the maximum surface erosion was acquired at the normal impingement angle (90°), however, mirrors exposed to natural aging presented lower surface erosion, probably due to erodent size and impact velocity. Bouzid et al. [27] also reported erosion results of sandblasting on the surface of soda-lime glass. The

experimental parameters were a constant erodent velocity of 16.6 m/s, sand grain sizes of 100 - 800 μm, and an impact angle ranging from 30 to 90°. It was reported that the weight loss rate increased proportionally with the increasing sand-blasting duration and impact angle approaching 90°.

Contrary to metals, there is a limited number of studies on non-metals, especially on transparent materials such as glasses in the literature. The erosive wear by sand particles for brittle materials like glass is a famous phenomenon in the Saharan region. Moreover, the progressive mass loss on surface glasses influenced both the mechanical properties and optical transmission [28]. Lallemant et al. [29] tested soda-lime glass and transparent ceramics such as alumina and magnesium-aluminate spinel materials against soda sand erosion and investigated their optical transmission behavior. They stated that surface roughness increased as the hardness of the target material decreased. As a result, optical transmission upon sand erosion is deteriorated due to increased surface roughness.

To understand the effect of the hardness of erodents on the erosion of target material, Feng et al. [30] used four target materials (glass, alumina, WC-7% Co and 304 stainless steel), and seven different erodents (steel shot, glass beads, silica, alumina, tungsten carbide, silicon carbide, and diamond) 63 to 1000 μm in particle diameters. The tests were conducted at impact angles of 30 and 90° and erodent particle velocities of 33, and 99 m/s, respectively. For brittle materials like glass and alumina, the erosion rate is determined by the velocity, particle size, and relative hardness of erodents. However, the shape of the erodent and impact velocity significantly affected the erosion rate of ductile materials. It was also reported that the glass always exhibited poor erosion resistance in comparison with other materials. In another study, Zhou et al. [31] investigated the effect of impact angle, erodent type, and nano-silica content on the erosive wear characteristics of transparent nanocomposite coatings. All the tested samples, regardless of their nano silica content, showed a brittle erosion response. Besides, these kinds of polyacrylate-based coatings were found to be insensitive to sharped-edge particles due to their filler content. Solar panels were also tested against sand particle erosion by Humood et al. [32]. The effects of erodent corner radius, impact velocity, and glass types were systematically investigated, and an analytical model was established. Results showed enhancement in impact damage resistance of solar panels due to the applied tempering process. There are some modeling efforts of SPE in the literature, too [1,33–38]. Several other studies on the particle erosion behavior of different materials are available in the literature [39–44].

Different from existing studies in the literature, this study focuses on the solid particle erosion performance of transparent materials, which are widely used in the automotive, aerospace, and construction industries. The main objective of the study is not only to reveal the erosion resistance of relevant transparent materials but also to determine the variation in the erosion behavior of these materials under different process conditions (impact velocity, impact angle, etc.). The outcomes of this research can be used as a reference in material selection for the abovementioned industries.

2. MATERIALS AND METHODS

A commercially available Polycarbonate (PC) sample (SABIC Inc., Riyadh, Saudi Arabia) 5 mm in thickness, 8 mm thick Plexiglas (PG), and laminated glass (LG) material (Şişecam Corp., İstanbul, Türkiye) were used as materials of interest in the current study. The laminated glass samples used have a thickness of 8.38 mm upon combining two glasses 4 mm in thickness and 0.38 mm thick transparent polyvinyl butyral (PVB) adhesive interface between those. The specimens were cut in 30×30 mm^2 dimensions. The photos of tested samples are given in Fig. 1. All the materials were tested by using an in-house developed erosion test system whose schematic is given in Fig. 2-a and a part description is given in Fig. 2-b. The test system was developed per both ASTM G76-13 and MIL-STD-3033 test standards [45,46]. The test parameters are presented in Table 1.

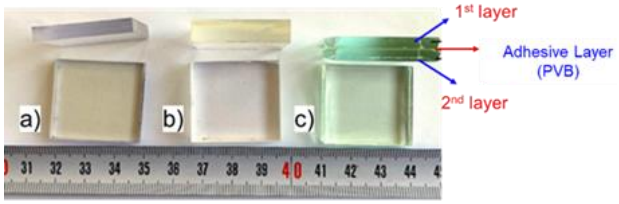

Fig. 1. Specimens before test, (a) Polycarbonate, (b) Plexiglass, (c) Laminated Glass.

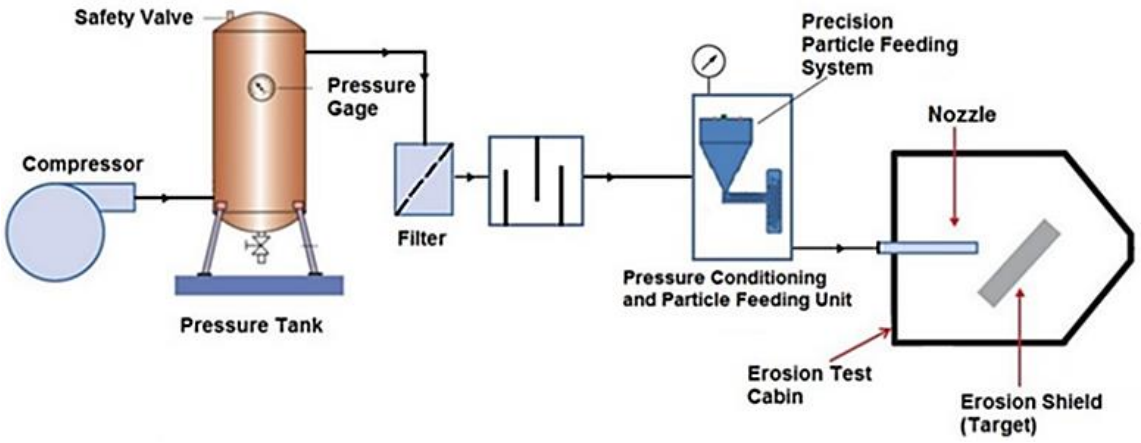

a)

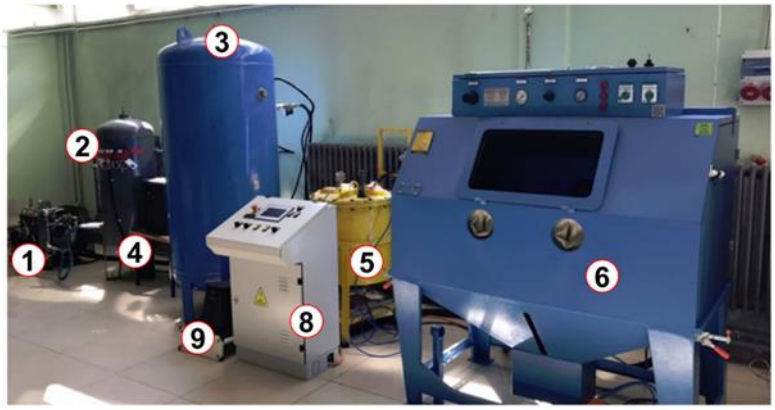

Components of Test System

1. Compressor
2. Pressure tank
3. Pressure reservoir (for higher capacity)
4. Pressurized air dryer
5. Pressure conditioning and particle feeding unit
6. Test Cabin
7. Moving platform actuated with step motors (Inside test cabin)
8. Test control unit
9. UPS

b)

(c)

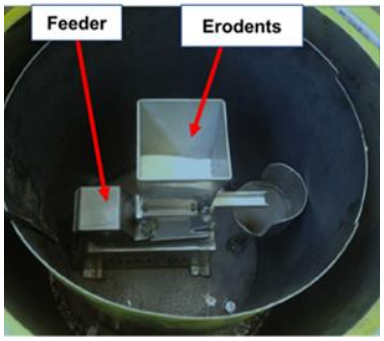

(d)

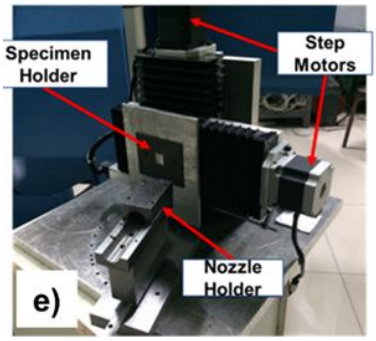

(e)

Fig. 2. Solid particle erosion test system, (a) Schematic of the test system, (b) Actual photo of the test system and its components, (c) Pressure conditioner and particle feeding unit, (d) Inside of the component 5, (e) Inside the test cabin (6).

Angular-shaped alumina (Al_2O_3) with 52 μm nominal diameter and two different angular-shaped silicon carbide (SiC) particles (71 μm and 348 μm in nominal diameter) were used as erodent particles. Scanning electron microscopy (SEM) images and particle size distributions of alumina and silicon carbide erodent particles are given in Fig. 4. The average erodent particle size for all erodent particles was measured with MasterSizer (Malvern Panalytical Inc., Malvern, UK).

Measurement and calibration of erodent particle velocities and corresponding air pressure values were determined by using the double-disc method suggested by Ruff and Ives [47]. The schematic representation of the double disc method is shown in Fig. 3. Two circular discs at a fixed distance and parallel to each other, one at the top (slotted) and one at the bottom rotate synchronously. The nozzle is positioned on the upper slotted disc at a certain distance. Then, while the discs are not rotating, abrasive particles at a certain pressure

are sprayed through the slots, leaving a reference mark on the lower disc. The same process is then carried out by rotating the discs. In this way, a second track is formed next to the previous reference mark. Afterward, the distance between the tracks is measured and the impact velocity of the abrasive particles is determined with the help of the equations (1-3) given below:

$$S = \theta * r \tag{1}$$

$$S = (\omega * t) * r = \left\{\left[\frac{2*\pi*n}{60}\right] * \left(\frac{L}{V}\right) * r\right\} \tag{2}$$

$$V = (2 * \pi * r * \omega L)/S \tag{3}$$

where;

s: distance between erosion marks [mm],

θ: angular displacement [rad],

r: average radius of erosion marks [mm],

ω: angular velocity [rad/s],

t: particle travel time between discs[s],

n: the revolution of the disks [rpm],

L: distance between discs [mm],

V: particle impact velocity [m/s].

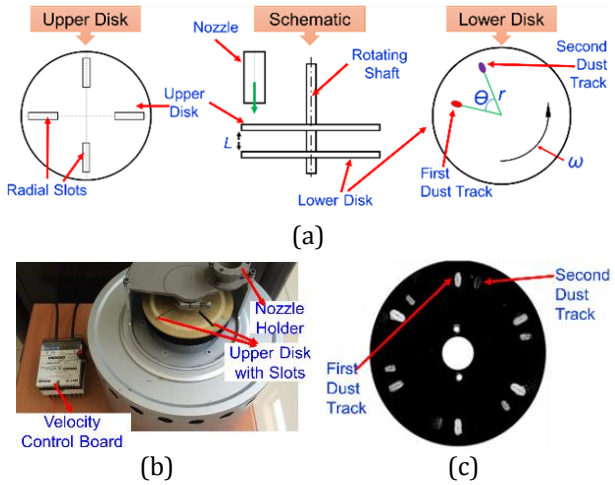

Fig. 3. Double-disk velocity measurement system, (a) Schematic and details of the device, (b) Photo of the actual device, (c) Lower disk with experimental dust tracks.

Calibrated corresponding air pressure values for each impact velocity and each erodent particle type and size are given in Table 2. The hardness of target materials was obtained from the average of five different measurements acquired from different points on the surface of materials using Duramin Microhardness tester (Struers, Denmark) with a load of 1.96 N for 10 seconds (Fig. 5). The hardness values of materials PG, PC, and LG were measured as 24.6 HV, 16.4 HV, and 564 HV, respectively (Table 3).

Following the weight measurements, the test samples were fixed to the frame shown in Fig. 2-e. The nozzle air outlet surface was set 10 mm away from the center of the surface of the specimen. Test parameters, such as gas pressure, erodent particle feed rate, and test duration were set using a digital touchscreen placed on the control panel (#6) shown in Figure 2-b. Once the planned test parameters were set, pressurized air was released through the nozzle. Afterward, the erodent particles were moved through the nozzle. The test is automatically interrupted at four-minute intervals (4x4=16 minutes, total test duration), and the weight of the test sample is measured at each interval at least three times to address the repeatability by using a digital electronic balance with 0.1 mg accuracy, and then an average value was reported.

Table 1. Solid particle erosion test parameters.

Test parameters	Values
Erodent & Size	Al_2O_3 (52 µm), SiC (71 µm and 348 µm)
Angle of impingement, α	20°, 30°, 45°, 60°, 90°
Erodent velocity, V	75, 150, 190, 200 m/s
Erodent feed & Air flow rate	2.5 g/min & 8 l/min
Duration of each test, t	4x4 = 16 minutes
Test temperature	Room temperature
Stand-off Distance	10 mm
Nozzle types & diameters	Convergent- divergent, d=1.6 mm- d=3.2 mm

The erosion wear rate was measured by Eq. (1) as follows:

$$E = \frac{m_1 - m_2}{\dot{m} \cdot t} \tag{4}$$

where,

E: erosion rate [g/g],

m_1: target material mass before the erosive wear test [g],

m_2: target material mass after the erosive wear test [g],

$\dot{m}$: erodent feed rate [g/min],

t : erosion test duration [min].

The erosion tests were performed in three stages as given in Table 4. The erosion exposure time was a total of 16 min (4x4 min) and at least three specimens were tested for each test condition to eliminate the error of discreteness. For the first two phases of testing, a 1.6 mm diameter nozzle was used. In the third stage, a

3.2 mm diameter nozzle (Fig. 3-g) was used to prevent blockage issues. In the first stage of testing, PC, PG, and LG samples were subjected to Al_2O_3 (52 µm) particles with a constant impact velocity of 150 m/s at different impact angles of 20°, 30°, 45°, 60°, and 90° to reveal the effect of impingement angle. In the second stage, the effect of kinetic energy on the erosion rate of samples was studied by using the same erodent particle (Al_2O_3) at various impact velocities of 75, 150, and 190 m/s at perpendicular incidence. Test results of the first two stages showed that the erosive resistance of PC material was relatively high when compared with the performances of the other two samples. Therefore, the third stage of testing was planned with PC samples to evaluate the performance of PC materials and the effect of the erosive particle size on the PC materials. To this goal, the PC material was tested against relatively harder and brittle particle SiC at an impact angle of 90° with different impact velocities (75, 150, and 200 m/s) using two different SiC erodent particle sizes (71 µm, and 348 µm).

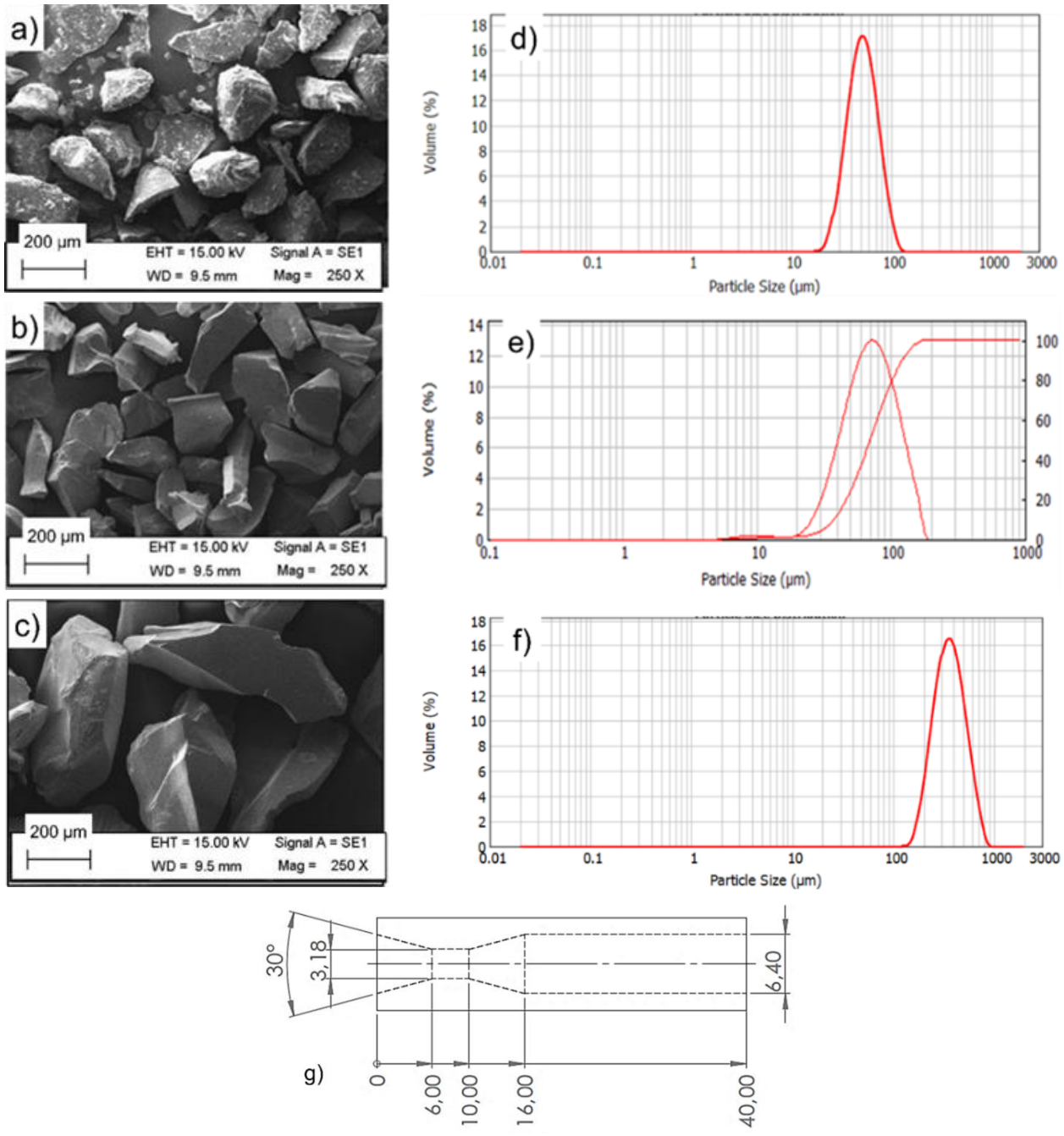

Fig. 4. SEM images, (a) Al_2O_3 - 52 µm, (b) SiC - 71 µm, (c) SiC - 348 µm, and particle size distributions, (d) Al_2O_3 - 52 µm, (e) SiC - 71 µm, (f) SiC - 348 µm, of erodent particles, and (g) dimensions of convergent-divergent nozzle used in the study.

Table 2. Erodent impact velocity and corresponding pressure values for each erodent particle type and size.

Erodent Particle	Impact Velocity (m/s)	75	150	190	200
Angular-shaped Alumina (52 µm)	Pressure (mbar)	300	2100	4000	N/A
Angular-shaped Silicon carbide (71 µm)		380	2030	N/A	3700
Angular-shaped Silicon carbide (348 µm)		1100	6630	N/A	11000

(a) (b) (c)

Fig. 5. Micro-Vickers hardness trace of materials, (a) Polycarbonate, (b)Plexiglass, (c) Laminated glass.

Table 3. Target materials' properties.

Target Materials	Hardness (HV)	Density (g/cm^3)
Laminated glass	564	2.5
Polycarbonate	16	1.19
Plexiglass	25	1.18

Table 4. Test specification.

Stages & Test Purposes	Target Materials	Test Parameters	Value
1 - Effect of impingement angle	PC, PG, LG	Impact Velocity (m/s)	150
		Impact Angle (°)	20, 30, 45, 60, 90
		Erodent	Al_2O_3 (52 µm)
2 - Effect of erodent velocity	PC, PG, LG	Impact Velocity (m/s)	75, 150, 190
		Impact Angle (°)	90°
		Erodent	Al_2O_3 (52 µm)
3- Effect of particle size	PC	Impact Velocity (m/s)	75, 150, 200
		Impact Angle (°)	90°
		Erodent (µm)	SiC (71 µm)
	PC	Impact Velocity (m/s)	75, 150
		Impact Angle (°)	90°
		Erodent	SiC (348 µm)

3. RESULTS AND DISCUSSION

3.1 Effect of erodent particle velocity

The variation of erosion rate with erodent impact velocity at perpendicular incidence is shown in Fig. 6. All the materials were tested against Al_2O_3 particles (52 µm) at different impact velocities which are 75, 150, and 190 m/s. As it can be noticed from Fig. 6, increasing abrasive erodent impact velocity gave rise to an increase in the erosion rate of materials. Polycarbonate exhibited a significant erosion resistance compared to the other tested samples. Laminated glass yielded the weakest erosion resistance at erodent velocities of 75 m/s, and 150 m/s and it was perforated upon 7 minutes of testing at an impact velocity of 190 m/s. In addition, Plexiglass performed better erosion resistance when compared to LG material at low velocities. Nevertheless, PG material was perforated upon 4.5 minutes of testing at 190 m/s impact velocity. Therefore, it exhibited the weakest erosion resistance at high abrasive impact velocity when compared with others.

Suresh et al. [48] investigated the erosion behavior of several high-performance polymers. They expressed a power law relation between erosion rate (E) and impact velocity (V) with the equation below:

$$E = K \cdot V^n \tag{5}$$

where K refers to a material constant, and n refers to the velocity exponent. They calculated the n values of the high-performance polymers in the range of 1.4-3 for an impact angle of 90° impingement angle. In another study, Pool et al. [49] noted that the n values of polymer materials

with ductile behaviour ranged between 2 and 3 while the brittle ones ranged between 3 and 5. Using the above-given equation and the least squares method, *K* and *n* values of PG, PG, and LG were calculated in the current study. The *K* values of PG, PC, and PG were calculated as $1.3x10^{-3}$, $2.73x10^{-6}$, and $28.9x10^{-3}$ while the *n* values were calculated as 2.1, 2.9, and 1.6, respectively. It is observed that these n values calculated for PG and PC are compatible with the n values given in the abovementioned studies. The smallest value of n was observed for LG, and the largest value was obtained for PC. When the trends of the curves are analyzed by taking any impact velocity value into account, it is noted that the highest erosion is for LG, and the least erosion is obtained with PC. Therefore, there is an increase in erosion resistance with the increasing n value.

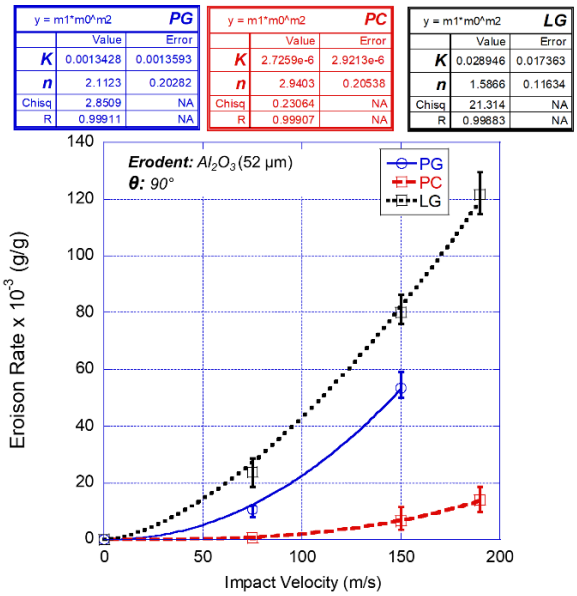

Fig. 6. Variation of erosion rate with impinging particle velocity upon 8 minutes of testing.

3.2 Effect of impingement angle

Fig. 7 shows the measured erosion rates of all materials at various impingent angles using the same abrasive erodent particles (Al_2O_3, 52 µm). The maximum erosion rate of polycarbonate occurred at an impingement angle of 30° which implies that PC exhibits ductile erosive behavior. In addition, the minimum erosion rate was obtained at 90° the impact angle. It is clear from Fig. 7 that PC material exhibits the best erosion resistance at all impingement angles. The maximum erosion rate of plexiglass was obtained at an angle of about 45° which revealed a semi-ductile behavior.

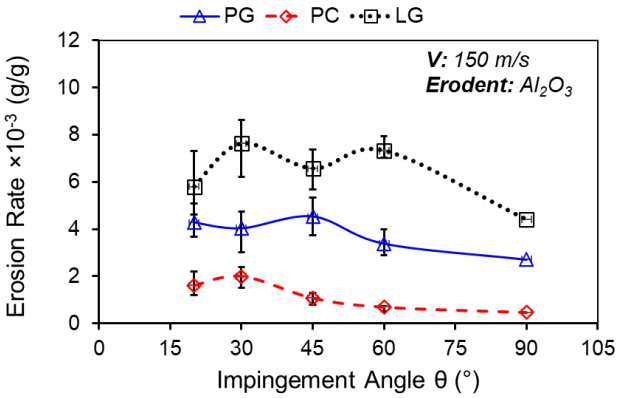

Fig. 7. Effect of impingement angle on erosion rate for all materials tested against Al_2O_3 (52 µm) erodent particles at 150 m/s impact velocity for 8 minutes of testing.

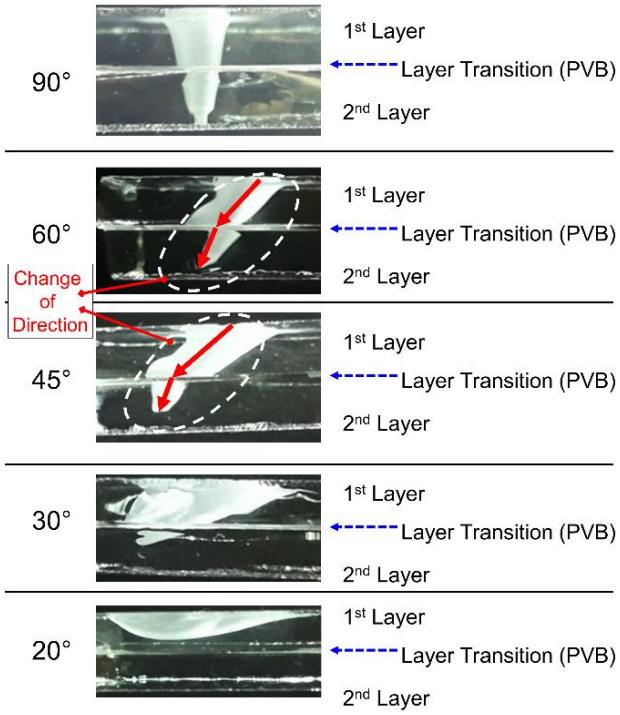

Fig. 8. Characteristics of particle erosion for laminated glass material at different impact angle conditions.

This is in agreement with the existing literature as it is stated that the maximum erosion is expected to occur at 60° for thermoset materials presenting a semi-ductile response [50,51]. Laminated glass material behaved slightly different due to the adhesive layer. The maximum erosion rate was noted at an impingement angle of 30° and the minimum erosion rate was achieved at 90° impact angle which implies that the LG material displays ductile erosive behavior. A similar trend was reported by Ismail et al. [52]. Similarly, Sheldon and Finnie [25] found that when particle size decreases, the erosion characteristic of glass gradually moves from brittle to ductile behavior. It is also important to note the role of the PVB layer between the glass

layers in the erosion rate. As it is presented in Fig. 8, the 0.38 mm thick PVB interlayer led to a delay in the erosion of LG at a 45° impingement angle. In addition, the erosion changed its direction from the impact angle to higher angles at 45° and 60° impact angle conditions due to the adhesive layer (PVB), as it can be noticed in Fig. 8.

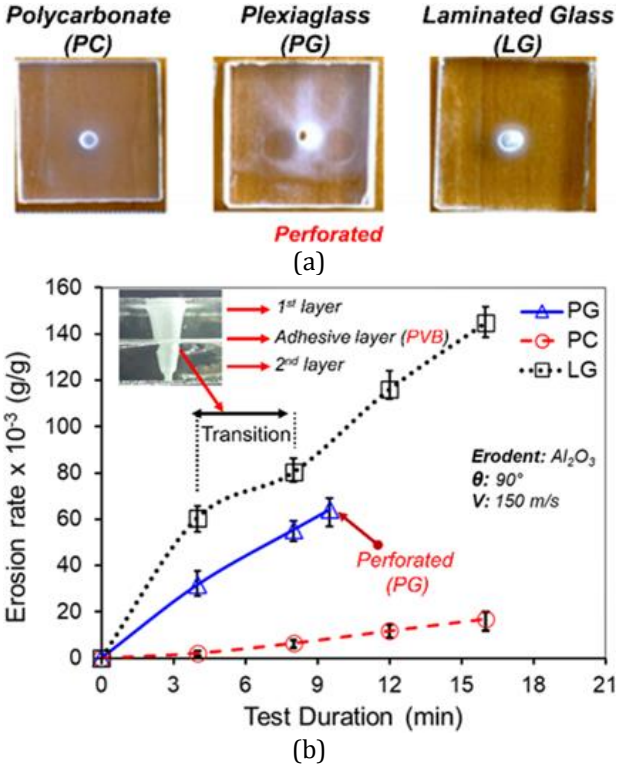

Fig. 9. (a) Samples subjected to testing at an impact angle of 90°, (b) erosion rate vs. test duration for tested materials (V = 150 m/s, θ = 90°, Al_2O_3 of 52 µm.)

Fig. 9-a shows the eroded samples while Fig. 9-b presents the erosion rate of all the tested materials at a 90° impingement angle, the erodent impact velocity of 150 m/s, and with an alumina erodent of 52 µm in nominal diameter with respect to test duration. The highest erosion resistance was obtained for PC material with an almost linear erosion trend. PG material exhibited a relatively high erosion resistance when compared with LG with a similar erosion trend as PC until 9.5 minutes of testing. Then, however, PG was perforated between 9-10 minutes of testing, as it can be noticed from Fig. 9. Laminated glass also exhibited a linear erosion trend except for testing of period 4-8th minutes which is the transition from the erosion of the upper layer to the lower layer. This disruption in linear trend was due to erosion of the PVB adhesive layer that was placed between laminates of glass. It retarded the erosion rate of LG till its complete removal.

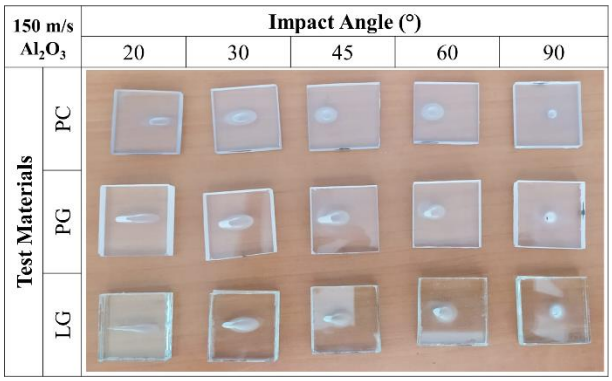

Fig. 10. Eroded samples surfaces upon testing at different impingement angles (V = 150 m/s, Al_2O_3 of 52 µm).

Eroded sample surfaces at different impingement angles upon testing against Al_2O_3 (52 µm) particles at 150 m/s impact velocity are tabulated in Fig. 10. The change of the erosion track with increasing impingement angle is clearly visible. Relatively longer and larger erosion traces are noted at impingement angles other than 90° yet the smallest but the deepest erosions were obtained at normal impingement angle, as expected.

3.3 Comparison of volumetric erosion rates

The volumetric erosion rate was calculated by the following equation [24];

$$E_v = \frac{V_r}{\dot{m} \cdot t} \tag{5}$$

where E_v is the volumetric erosion rate, V_r is the removed volume of target material, $\dot{m}$ is the erodent particle feed rate and t is the test duration.

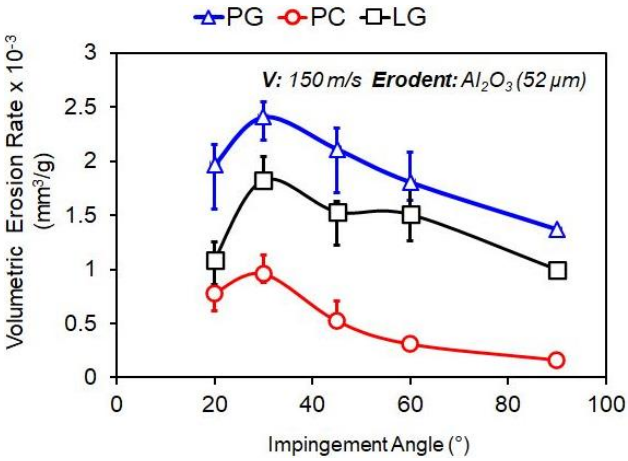

Fig. 11. The volumetric erosion rate of tested materials as a function of impingement angles (V = 150 m/s, t = 4 minutes, Al_2O_3 of 52 µm).

Fig. 11 shows the volumetric erosion rate performance of tested materials at an erodent

impact velocity of 150 m/s at various impingement angles. Again, the PC material exhibited a superior volumetric erosion performance compared to others. It was also noted that PG yielded the weakest volumetric erosion performance among the tested materials which is different from the first stage of testing.

3.4 Erosion efficiency

The erosion efficiency η is used to define the nature and mechanism of erosion wear which is described as the fraction of the volume of materials that is removed as erosion debris out of that which is displaced. It is given by the following equation [53,54]:

$$\eta = \frac{2 \cdot H \cdot E}{\rho \cdot v^2} \quad (6)$$

where E is the erosion rate, H is the hardness of the target material, ρ is the density of the target material, and v is the velocity of abrasive erodent particles. However, if the erosion rate is defined in terms of volume loss per unit mass of erodent, the equation can be converted into the following form:

$$\eta = \frac{2 \cdot H \cdot E_v}{v^2} \quad (7)$$

It is noted that the above equations are especially valid for perpendicular incidence only and used in terms of identifying the erosion mechanism (brittle or ductile) of materials. For example, ideal micro-ploughing involving just the displacement of materials without any erosion wear will result in η = 0. For an ideal micro-cutting, η is 1 or 100%. For ductile materials, erosion efficiency is in the range of 0-100%. In the case of brittle materials, erosion wear usually occurs by spalling and removal of large chunks of materials by interlinking of lateral or radial cracks, and thus η is greater than 100% [53,54].

The values of erosion efficiency of materials are calculated using Eq. (6) and are given in Table 5. It is noted from Table 5 that erosion efficiency increases with increasing hardness. Thus, the harder the material larger the fraction of the crater volume [52]. The PC materials indicated a ductile performance with η from 0.31 to 1.06% at impact velocities of 75 to 190 m/s, respectively. The PG materials presented a ductile behavior, too and its η ranged from 7.87 to 9.89% with 75 and 150 m/s impact velocities, respectively. The LG material showed a brittle performance as it was expected and its erosion efficiency varies from 190.94 to 152.13% at impact velocities of 75 to 190 m/s, respectively. Here, one aspect that merits attention regarding LG is increasing impact velocity changed the characteristics of the material (brittle to ductile).

Table 5. Erosion efficiencies of tested materials.

Materials	η (%)		
	V= 75 m/s	V=150 m/s	V=190 m/s
PC	0.31	0.79	1.1
PG	7.9	9.89	-
LG	190.6	160.9	152.1

In Fig. 12, the erosion index of test materials is illustrated. PC is 12 times more resistant to erosive wear compared to PG and 18 times more resistant compared to LG.

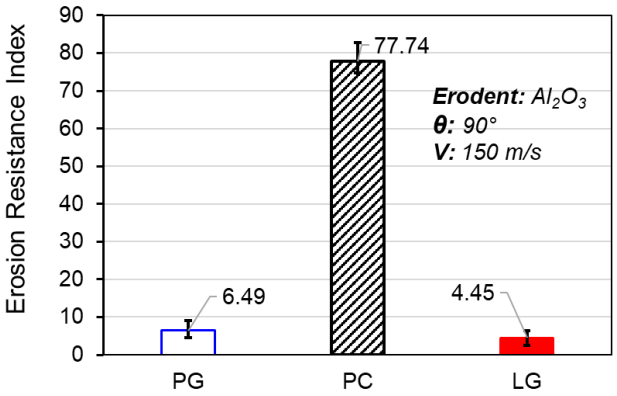

Fig. 12. Erosion index of tested materials (V = 150 m/s, θ = 90° , Al_2O_3 of 52 µm).

3.5 Effect of erodent particle size

In this last stage of experiments, polycarbonate samples were subjected to erosion tests against SiC particles with two distinct sizes in particle diameter. The primary reason for choosing PC material as the only material is its superior erosion wear behavior when compared to other tested transparent materials. At this stage, the erosion rate of PC has been studied by varying SiC erodent sizes of 71 µm and 348 µm at various impact velocities (75 m/s, 150 m/s), at an impingement angle of 90°.

Fig. 13 shows the effect of the erodent type and particle size on the erosion rate of polycarbonate material upon 16 minutes of testing. Considering the erosion rates due to SiC erodent particles, it is observed that erosion wear increases with increasing erodent particle size, drastically.

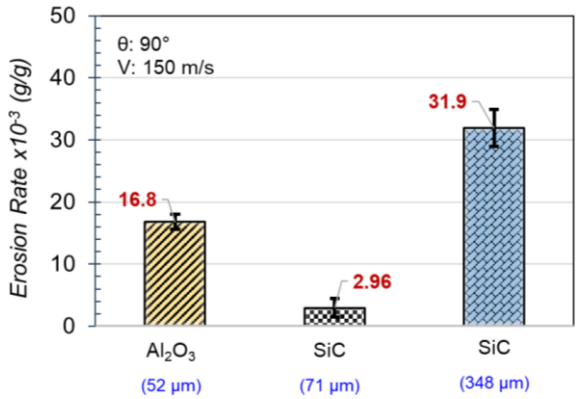

Fig. 13. Effect of erodent type and size on the performance of Polycarbonate material.

As illustrated in Fig. 14, the bigger abrasive erodent particle size caused a higher erosion rate. In other words, the size of the erodent particle significantly affects the erosion rate, and this result is in parallel with the existing literature [23,55]. Another important trend was the formation of incubation zones regardless of particle speed. Moreover, the incubation period and embedment of erodent particles onto the target material surface were observed for the tests performed using SiC-71 µm erodent particles. The incubation period-I lasted till the 7th minute of testing, and then erosive wear continued to linearly increase as usual. Because of the lower erodent velocity, the incubation period-II lasted 12 minutes of testing.

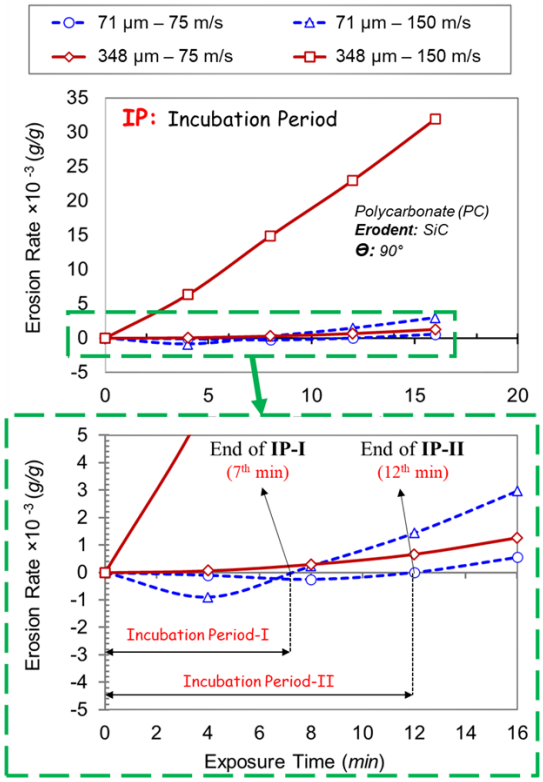

Fig. 14. The effect of erodent particle size on the erosion rate of Polycarbonate at different impact velocities (70, 150 m/s), and at θ = 90°.

4. CONCLUSION

Transparent materials are used in a variety of fields including machinery (e.g., transparent cabins of test/manufacturing systems), construction (e.g., buildings' façade, roofs, etc.), automotive (e.g., windshield), and aeronautics (e.g., canopy) industries, etc. Those materials are subjected to solid particle erosion due to their working environments. In the current study, the solid particle erosion performance of three different transparent materials, namely polycarbonate (PC), plexiglass (PG), and laminated glass (LG) were evaluated under different test conditions, e.g., impact velocity, impact angle, and erodent particle size.

Within the limitation of the study, it was noted that the erosion of investigated materials increased with increasing impact velocity due to the increased kinetic energy of erodent particles. Laminated glass against Al_2O_3 erodent particles exhibited ductile behavior regardless of impact velocity adopted whereas plexiglass showed semi-ductile behavior. Change in the direction of erosion was observed for the laminated glass at 20° and 30° impact angles due to the polyvinyl butyral (PVB) layer in between the laminates. This PVB layer changed the linear behavior and delayed erosion wear, noticeably. Polycarbonate samples were the thinnest ones among the tested materials yet those outperformed both plexiglass and laminated glass regardless of impact velocity and impact angle. Polycarbonate was the only material that was not perforated even at 190 m/s impact speed of erodent particles. An incubation phenomenon, which contributes to polycarbonate's erosion performance positively, was observed during the initial period of erosion tests performed with SiC particles. Besides, polycarbonate exhibited a ductile behavior while its peak erosion and minimum erosion values were obtained at impact angles of 30° and 90°, respectively. It was concluded that polycarbonate was at least 17 times more resistant to solid particle erosion than laminated glass and 12 times more durable compared to plexiglass.

Acknowledgments

The authors are thankful for the project support from the Rotary Wing Technology Center - Turkish Aerospace Industries (Project # DKTM/2015-03, PI: Prof. Hasan GEDİKLİ) through which the solid particle erosion test system was constructed.

REFERENCES

[1] N. H. Arani, M. Eghbal, and M. Papini, "Numerical simulation of solid particle erosion of epoxy by overlapping angular particle impacts," *Tribology Letters*, vol. 68, no. 2, Apr. 2020, doi: 10.1007/s11249-020-01305-w.

[2] C. Samuel, M. Arivarasu, and P. Ram, "High-Temperature solid particle erosion behavior of laser powder bed fused Inconel 718," *Journal of Tribology*, vol. 144, no. 9, Mar. 2022, doi: 10.1115/1.4054052.

[3] M. Al-Bukhaiti, A. Abouel-Kasem, K. M. Emara, and S. M. Ahmed, "Particle shape and size effects on slurry erosion of AISI 5117 steels," *Journal of Tribology*, vol. 138, no. 2, Jan. 2016, doi: 10.1115/1.4031987.

[4] A. Abouel-Kasem, "Particle Size Effects on Slurry Erosion of 5117 steels," *Journal of Tribology*, vol. 133, no. 1, Dec. 2010, doi: 10.1115/1.4002605.

[5] K. Shu *et al.*, "Study on the influence of sand erosion process on the wear and damage of Heat-Treated U75V Rail Steel," *Journal of Tribology*, vol. 143, no. 8, Dec. 2020, doi: 10.1115/1.4049110.

[6] N. M. Barkoula, J. K. Kocsis, "Review processes and influencing parameters of the solid particle erosion of polymers and their composites," *Journal of Materials Science*, vol. 37, pp. 3807–3820, doi: 10.1023/A:1019633515481.

[7] M. Du, Z. Li, X. Dong, C. Fan, J. Che, and Y. Zhang, "Experiment and simulation of erosion behavior and deformation characteristics in AL6061-T6 beam due to rhomboid particle impacts," *Tribology Letters*, vol. 69, no. 3, Jun. 2021, doi: 10.1007/s11249-021-01465-3.

[8] M. C. Park, K. N. Kim, J. Y. Yun, G. S. Shin, and S. J. Kim, "Strain-Induced ε/α′ Martensitic Transformation Behavior and Solid Particle Erosion Resistance of Austenitic Fe–Cr–C–Mn/Ni Alloys," *Tribology Letters*, vol. 54, no. 1, pp. 51–58, Feb. 2014, doi: 10.1007/s11249-014-0306-3.

[9] I. Finnie, "Some reflections on the past and future of erosion," *Wear*, vol. 186–187, pp. 1–10, Jul. 1995, doi: 10.1016/0043-1648(95)07188-1.

[10] B.G. Babu, P.N. Karthikeyan, K. Siva, C. Sabarinathan, "Study of erosion characteristics of MWCNT's-alumina hybrid epoxy nanocomposites under the influence of solid particles," Digest Journal of Nanomaterials and Biostructures, vol. 11, pp. 1367-1373, 2016.

[11] M. Kaplan, M. Uyaner, E. Avcu, Y. Y. Avcu, and A. C. Karaoğlanlı, "Solid particle erosion behavior of thermal barrier coatings produced by atmospheric plasma spray technique," *Mechanics of Advanced Materials and Structures*, vol. 26, no. 19, pp. 1606–1612, Mar. 2018, doi: 10.1080/15376494.2018.1444221.

[12] Md. A. Islam and Z. Farhat, "Effect of impact angle and velocity on erosion of API X42 pipeline steel under high abrasive feed rate," *Wear*, vol. 311, no. 1–2, pp. 180–190, Mar. 2014, doi: 10.1016/j.wear.2014.01.005.

[13] G. Sundararajan and M. Roy, "Solid particle erosion behaviour of metallic materials at room and elevated temperatures," *Tribology International*, vol. 30, no. 5, pp. 339–359, May 1997, doi: 10.1016/s0301-679x(96)00064-3.

[14] N. Gat and W. Tabakoff, "Some effects of temperature on the erosion of metals," *Wear*, vol. 50, no. 1, pp. 85–94, Sep. 1978, doi: 10.1016/0043-1648(78)90247-8.

[15] É. Bousser, L. Martinů, and J. E. Klemberg-Sapieha, "Effect of erodent properties on the solid particle erosion mechanisms of brittle materials," *Journal of Materials Science*, vol. 48, no. 16, pp. 5543–5558, Apr. 2013, doi: 10.1007/s10853-013-7349-y.

[16] A. A. Erdoğan, E. Feyzullahoğlu, S. FiDan, and T. Sınmazçelik, "Determination of plastic deformation rate after solid particle erosion in ductile materials," *MP MATERIALPRUEFUNG - MP MATERIALS TESTING*, vol. 63, no. 12, pp. 1142–1149, Dec. 2021, doi: 10.1515/mt-2021-0054.

[17] B. Lindsley and A. R. Marder, "The effect of velocity on the solid particle erosion rate of alloys," *Wear*, vol. 225–229, pp. 510–516, Apr. 1999, doi: 10.1016/s0043-1648(99)00085-x.

[18] P. C. Okonkwo, A. Mohamed, and E. Ahmed, "Influence of particle velocities and impact angles on the erosion mechanisms of AISI 1018 steel," *Advanced Materials Letters*, vol. 6, no. 7, pp. 653–659, Jul. 2015, doi: 10.5185/amlett.2015.5645.

[19] M. Roy, B. Vishwanathan, and G. Sundararajan, "The solid particle erosion of polymer matrix composites," *Wear*, vol. 171, no. 1–2, pp. 149–161, Jan. 1994, doi: 10.1016/0043-1648(94)90358-1.

[20] Y. Q. Wang, L.-F. Huang, W. L. Liu, and J. Li, "The blast erosion behaviour of ultrahigh molecular weight polyethylene," *Wear*, vol. 218, no. 1, pp. 128–133, Jun. 1998, doi: 10.1016/s0043-1648(97)00289-5.

[21] S.M. Walley, J.E. Field, "The erosion and deformation of polyethylene by solid-particle impact, Philosophical Transactions of Royal Society London Series A," *Mathematical and Physical Sciences*, vol. 321, pp. 277-303, 1987, doi: 10.1098/rsta.1987.0016.

[22] M. Bağcı, H. İmrek, and A. Aktaş, "Solid particle erosion behaviour of glass mat-based polyester laminate composite materials," *Journal of Thermoplastic Composite Materials*, vol. 26, no. 6, pp. 777–794, Dec. 2011, doi: 10.1177/0892705711429490.

[23] A.M. Amaro, A.J.R. Loureiro, M.A. Neto, P.N.B. Reis, "Residual impact strength of glass/epoxy composite laminates after solid particle erosion," *Composite Structures*, vol. 238, 2020, doi: 10.1016/j.compstruct.2020.112026.

[24] N. H. Arani, W. Rabba, and M. Papini, "Solid particle erosion of epoxy matrix composites reinforced by Al2O3 spheres," *Tribology International*, vol. 136, pp. 432–445, Aug. 2019, doi: 10.1016/j.triboint.2019.04.010.

[25] G. L. Sheldon and I. Finnie, "On the Ductile Behavior of Nominally Brittle Materials During Erosive Cutting," *Journal of Engineering for Industry*, vol. 88, no. 4, pp. 387–392, Nov. 1966, doi: 10.1115/1.3672666.

[26] M. Karim, S. Naamane, C. Delord, and A. Bennouna, "Study of the surface damage of glass reflectors used in concentrated solar power plants," *Energy Procedia*, vol. 69, pp. 106–115, May 2015, doi: 10.1016/j.egypro.2015.03.013.

[27] S. Bouzid and N. Bouaouadja, "Effect of impact angle on glass surfaces eroded by sand blasting," *Journal of the European Ceramic Society*, vol. 20, no. 4, pp. 481–488, Apr. 2000, doi: 10.1016/s0955-2219(99)00140-5.

[28] C. Bousbaa, N. Iferroudjene, S. Bouzid, M. Madjoubi, N. Bouaouadja, "Effects of duration of sand blasting on the properties of window glass," *Glass Technology*, vol. 39, no. 1, pp. 24-26, 1998.

[29] L. Lallemant, V. Garnier, G. Bonnefont, A. Marouani, G. Fantozzi, and N. Bouaouadja, "Effect of solid particle impact on light transmission of transparent ceramics: Role of the microstructure," *Optical Materials*, vol. 37, pp. 352–357, Nov. 2014, doi: 10.1016/j.optmat.2014.06.025.

[30] Z. Feng and A. Ball, "The erosion of four materials using seven erodents — towards an understanding," *Wear*, vol. 233–235, pp. 674–684, Dec. 1999, doi: 10.1016/s0043-1648(99)00176-3.

[31] L. Zhou, H. Zhou, X.-Q. Pei, K. Friedrich, C. Eger, and Z. Zhang, "Erosive wear of transparent nanocomposite coatings," *Tribology International*, vol. 61, pp. 62–69, May 2013, doi: 10.1016/j.triboint.2012.11.021.

[32] M. Humood, A. Beheshti, J. L. Meyer, and A. A. Polycarpou, "Normal impact of sand particles with solar panel glass surfaces," *Tribology International*, vol. 102, pp. 237–248, Oct. 2016, doi: 10.1016/j.triboint.2016.05.022.

[33] V. Hadavi, N. H. Arani, and M. Papini, "Numerical and experimental investigations of particle embedment during the incubation period in the solid particle erosion of ductile materials," *Tribology International*, vol. 129, pp. 38–45, Jan. 2019, doi: 10.1016/j.triboint.2018.08.013.

[34] V. Hadavi and M. Papini, "Numerical modeling of particle embedment during solid particle erosion of ductile materials," *Wear*, vol. 342–343, pp. 310–321, Nov. 2015, doi: 10.1016/j.wear.2015.09.008.

[35] J. Kumar, G. Tiwari, A. Rawat, and V. K. Patel, "Computational investigation of erosion wear on industrial centrifugal pump handling Solid-Water flows," *Tribology in Industry*, vol. 42, no. 3, pp. 382–399, Sep. 2020, doi: 10.24874/ti.803.11.19.06.

[36] B. Mohammadi, A. Khoddami, and M. Pourhosseinshahi, "Numerical and experimental investigation of erosive wear of TI-6AL-4V alloy," *Journal of Tribology*, vol. 141, no. 10, Aug. 2019, doi: 10.1115/1.4044298.

[37] N. Banazadeh-Neishabouri and S. A. Shirazi, "Development of erosion equations for Fiberglass Reinforced Plastic (FRP)," *Wear*, vol. 476, p. 203657, Jul. 2021, doi: 10.1016/j.wear.2021.203657.

[38] M. Takaffoli and M. Papini, "Finite element analysis of single impacts of angular particles on ductile targets," *Wear*, vol. 267, no. 1–4, pp. 144–151, Jun. 2009, doi: 10.1016/j.wear.2008.10.004.

[39] D. Acar, S.L. Aktuğ, K. Korkmaz, S. Durdu, Ö.N. Cora, *Solid particle erosion performance of micro-arc oxidation and electro spark deposition coated Ti6Al4V sheets*, International Journal of Materials and Engineering Technology, vol. 5, iss. 1, pp. 28-32, Apr. 2022.

[40] D. Acar, D. Meriç, H. Sofuoğlu, R. Gümrük, Ö.N. Cora, H. Gedikli, *Design and manufacture of a test rig to examine solid particle erosion occurring on the helicopter blade wear shield*, in VI National Aeronautics and Space Conference, 28-30 September, 2016, UHUK, Kocaeli, Turkey, pp. 1–13. (In Turkish)

[41] S. More, D. V. Bhatt, and J. Menghani, "Study of the Parametric Performance of Solid Particle Erosion Wear under the Slurry Pot Test Rig," *Tribology in Industry*, vol. 39, no. 4, pp. 471–481, Dec. 2017, doi: 10.24874/ti.2017.39.04.06.

[42] Z. Fuadi, R. Kurniawan, and F. Mulana, "Tribo-layer properties on AISI52100 lubricated by palm methyl ester containing graphene nanosheet," *Tribology in Industry*, vol. 45, no. 1, pp. 191–200, Jun. 2023, doi: 10.24874/ti.1372.09.22.03.

[43] B. Öztürk, H. Gedikli, and Y. S. Kılıçarslan, "Erosive wear characteristics of E-glass fiber reinforced silica fume and zinc oxide-filled epoxy resin composites," *Polymer Composites*, vol. 41, no. 1, pp. 326–337, Aug. 2019, doi: 10.1002/pc.25372.

[44] D. Acar, Ö.N. Cora, *Solid particle erosion performance evaluation of Ti-6Al-4V as erosion shield material of a helicopter rotor blade*, in the Proceedings of 1st International Symposium on Light Alloys and Composites Materials, 22-24 March, 2018, IDLSC'18, Karabük, Türkiye, pp. 109-110.

[45] ASTM G76-07, *Standard test method for conducting erosion tests by solid particle impingement using gas jets*, 2013.

[46] MIL-STD-3033, *Particle/Sand erosion testing of rotor blade protective materials*, Department of Defense Test Method Standard, 2010.

[47] A. W. Ruff and L. K. Ives, "Measurement of solid particle velocity in erosive wear," *Wear*, vol. 35, no. 1, pp. 195–199, Nov. 1975, doi: 10.1016/0043-1648(75)90154-4.

[48] S. Arjula, A. P. Harsha, and M. Ghosh, "Solid-particle erosion behavior of high-performance thermoplastic polymers," *Journal of Materials Science*, vol. 43, no. 6, pp. 1757–1768, Mar. 2008, doi: 10.1007/s10853-007-2405-0.

[49] K. V. Pool, C. K. H. Dharan, and I. Finnie, "Erosive wear of composite materials," *Wear*, vol. 107, no. 1, pp. 1–12, Jan. 1986, doi: 10.1016/0043-1648(86)90043-8.

[50] N. Miyazaki and N. Takeda, "Solid particle erosion of fiber reinforced plastics," *Journal of Composite Materials*, vol. 27, no. 1, pp. 21–31, Jan. 1993, doi: 10.1177/002199839302700102.

[51] J. Zahavi and G. F. Schmitt, "Solid particle erosion of reinforced composite materials," *Wear*, vol. 71, no. 2, pp. 179–190, Sep. 1981, doi: 10.1016/0043-1648(81)90337-9.

[52] J. Ismail, F. Zaïri, M. Naït-Abdelaziz, S. Bouzid, and Z. Azari, "Experimental and numerical investigations on erosion damage in glass by impact of small-sized particles," *Wear*, vol. 271, no. 5–6, pp. 817–826, Jun. 2011, doi: 10.1016/j.wear.2011.03.009.

[53] G. Sundararajan, M. Roy, and B. Venkataraman, "Erosion efficiency-a new parameter to characterize the dominant erosion micromechanism," *Wear*, vol. 140, no. 2, pp. 369–381, Nov. 1990, doi: 10.1016/0043-1648(90)90096-s.

[54] H. Jena, A. K. Pradhan, and M. K. Pandit, "Study of Solid Particle Erosion Wear Behavior of Bamboo Fiber Reinforced Polymer Composite with Cenosphere Filler," *Advances in Polymer Technology*, vol. 37, no. 3, pp. 761–769, Jun. 2016, doi: 10.1002/adv.21718.

[55] A. V. S. S. K. S. Gupta, A. Kumar, A. Patnaik, and S. Biswas, "Effect of different parameters on mechanical and erosion wear behavior of bamboo fiber reinforced epoxy composites," *International Journal of Polymer Science*, vol. 2011, pp. 1–10, Jan. 2011, doi: 10.1155/2011/592906.